Investigating the Potential of Using Off-Axis 3D Woven Composites in Composite Joints' Applications

Mohamed Nasr Saleh[1] · **Ying Wang**[2] · **Arief Yudhanto**[3] ·
Adam Joesbury[1,4] · **Prasad Potluri**[1] · **Gilles Lubineau**[3] ·
Constantinos Soutis[4]

Abstract The effect of circular notch has been evaluated for three different architectures of three-dimensional (3D) carbon fibre woven composites (orthogonal, ORT; layer-to-layer, LTL; angle interlock, AI) through open-hole quasi-static tension and double-lap bearing strength tests in the off-axis (45°) direction. Damage characterisation is monitored using Digital Image correlation (DIC) for open-hole testing and X-ray Computed Tomography (CT) for double-lap bearing strength test. The off-axis notched 3D woven composites exhibits minor reduction (less than 10 %) of the notched strength compared to the un-notched strength. DIC strain contour clearly show stress/strain localisation regions around the hole periphery and stress/strain redistribution away from the whole due to the z-binder existence, especially for ORT architecture. Up to 50 % bearing strain, no significant difference in the bearing stress/bearing strain response is observed. However when ORT architecture was loaded up to failure, it demonstrates higher strain to failure (~140 %) followed by AI (~105 %) and lastly LTL (~85 %). X-ray CT scans reveal the effect of the z-binder architecture on damage evolution and delamination resistance. The study suggests that off-axis loaded 3D woven composites, especially ORT architecture, has a great potential of overcoming the current challenges facing composite laminates when used in composite joints' applications.

✉ Mohamed Nasr Saleh
   mohamed.uom@gmail.com

✉ Constantinos Soutis
   constantinos.soutis@manchester.ac.uk

[1] Northwest Composite Centre, School of Materials, University of Manchester, Manchester M13 9PL, UK

[2] Henry Moseley X-ray Imaging Facility, School of Materials, University of Manchester, Manchester M13 9PL, UK

[3] Physical Sciences and Engineering Division, COHMAS Laboratory, King Abdullah University of Science and Technology (KAUST), Thuwal 23955-6900, Saudi Arabia

[4] Aerospace Research Institute, University of Manchester, Manchester M1 3NJ, UK

Springer

1 Introduction

Although composite laminates are characterised by high stiffness and strength to weight ratio (high specific stiffness and high specific strength), in real life application where joining structures made of composites laminates is essential, the ultimate strength and stiffness of the structure is determined by the joint strength and joining efficiency [1]. Mainly there are two different joining techniques for composite laminates, namely bonded joints and mechanically fastened joints; which are mainly achieved by bolting. Sometimes both techniques are combined to form bonded-bolted joints [2]. Several requirements for a successful joint design in service include:

– Material ductility/yielding

  Composite materials are significantly less ductile than the types of metals used for similar structural. The stress, usually, cannot be distributed around a stress concentration region such as a notch or a hole, which is common in joints.
– Notch insensitivity

  The ultimate strength and stiffness of the metallic materials are not significantly affected by notches or drilling holes. On the contrary, composite laminates exhibit approximately 50 % reduction in strength as compared to their un-notched strength.
– High strain to failure and energy absorption

  As composite materials are brittle by nature, the energy absorbed up to final failure and strain to failure is relatively small especially if the material is loaded along the fibre direction.

These previously highlighted challenges make composite materials more susceptible to damage and joint problems once in service especially with regards to inspection. The weaknesses of composite laminates in the in-plane shear, transverse and inter-laminar shear drive the design of composites to rely mainly on the notched (reduced) properties instead of utilising the un-notched excellent properties. Research has been done to address some of the highlighted issues, such as the notch sensitivity and stress redistribution. In order to alleviate the stress concentration around holes in composite laminates, two methods were proposed and reported in [1]. The first method is referred to as Softening Strip method [3] in which a strip of a relatively softer composite, several times the hole diameter, is inserted around the hole/notch. In this case, the less stiff inserted material helps reducing the stress concentration around the hole but there is no control on the load redistribution. On the contrary, the second method is called Stiffening Strip method [1]. In this method, a relatively stiffer material is inserted away from the hole so that the load is attracted to that specific region. In the following section, types of composites joints and their design considerations are discussed.

Previous studies focused on evaluating the effect of notches on the fracture toughness, strength as well as damage and failure mechanisms of both laminated [4, 5] and 2D woven composites [6, 7]. It was observed that the woven laminates exhibited more resistance to delamination and splitting compared to laminated composites. The undulating nature of the woven fabric acted as crack stoppers in the sense that it prevented crack propagation within the matrix. This led to a notched strength that is higher for 2D woven laminates, compared to laminated composites, which can be interpreted as less notch sensitivity [8, 9]. Further

enhancement for the notch strength and fracture toughness of composites was achieved by replacing 2D woven by 3D woven composites as reported in [10, 11]. The through-thickness binder in 3D woven composites dramatically reduced the notch sensitivity of 3D woven composites and improved the fracture toughness and damage tolerance compared to 2D woven laminates. One recent study, by Dai et al. [12], investigated the notch sensitivity of CFRP composites of 3D orthogonal and 3D angle interlock woven composites tested in quasi-static tension and tension-tension fatigue. Both test categories focused on the on-axis loading; either along the warp or the weft direction. Damage evolution was characterised and monitored using DIC for quasi-static tension testing and infra-red camera for the fatigue testing. Moreover, the effect of the notch size was addressed by comparing two different hole sizes with a diameter to width ratio of 1/6 and 1/2 respectively. The study concluded that regardless of the hole size, the reduction in the strength of the investigated architectures did not exceed 17 % compared to the un-notched strength in the case of on-axis loading. Although 3D woven composites tested along the warp or weft directions have been proven to be relatively notch insensitive [12, 13], nothing was reported with regards to the behaviour/sensitivity of 3D woven composites loaded along the off-axis direction.

In spite of many studies investigating the bearing response of 2D laminated composites [14–21], the literature discussing the bearing response for 3D woven composites is quite sparse. Only one recent study by Warren et al. [22] investigated the bearing response of two 3D woven architectures namely as layer-to-layer and orthogonal. The study extensively investigated the single-lap bearing response of these architectures and its dependency on the loading orientation using seven different orientations between warp (0°) and weft (90°) directions. In addition, the study focused on the double-lap bearing response of the same architectures along the warp direction. For the layer-to-layer architecture, two sizes of IM7 carbon tows were used 12 k and 24 k respectively. The study concluded that 3D woven composites fail in non-catastrophic manner and the associated failure mode is bearing failure. The most dominant damage mechanisms were found to be matrix cracking and tow distortion around the hole which caused some drop in the load. Changing the loading direction orientation in the single-lap bearing strength test led to stiffness reduction in the range of 24.7 % to 32.7 % of the on-axis stiffness. The 24 k tow size increased slightly the bearing response compared to 12 k layer-to-layer and orthogonal architecture.

Thus, the objective of this study is to investigate the potential of utilising the off-axis loaded 3D woven composites in design of composite joints through two main tests (open-hole tension and double-lap bearing strength). The paper is divided into five sections. Section 2 details the 3D woven architectures, composite manufacturing and cutting processes. Section 3 describes the specimens' preparation process and test setup (open-hole tensile test and double-lap bearing strength). Section 4 details the results and discusses the significance of the experimental observations (effect of z-binder on the notch sensitivity and the bearing response of 3D woven composites tested in the off-axis direction as well as damage progression). Finally, section 5 summarises the main concluding remarks of the paper suggesting the potential of utilising 3D woven composites in composite joints' applications.

2 Materials and Manufacturing

The carbon fibre, used in this study, is HexTow IM7 (Hexcel), while the epoxy is MTM 57 (medium temperature epoxy produced by Solvay). The 3D woven dry fabrics are produced by

Sigmatex UK. Three architectures are investigated, namely orthogonal (ORT), layer-to-layer (LTL) and angle interlock (AI). Figure 1 shows the schematic architecture of the three 3D woven fabrics drawn using TexGen software. Specification of the textile architecture parameters of 3D woven composites are detailed in Table 1. Warp and weft fibre count for ORT, AI and LTL is 12 k. The z-binder fibre count for ORT, AI and LTL is 6 k, 6 k and 12 k, respectively. The number of warp threads, weft threads and z-binder threads per unit length (centimetre) is specified in Table 1 as ends/cm, picks/cm and binders/cm, respectively. In addition, the areal density of the dry 3D woven fabric is also given in Table 1 (unit is g/m^2).

To produce 3D woven composite panels, the dry fabrics were infused by MTM 57 epoxy matrix using resin film infusion (RFI) process. Infusion process was carried out at 70 °C for 1 h, while curing process was done at 120 °C for 1 H. *minimum* curing pressure for MTM 57 was set to 2.8 bars. Once the 3D woven composite panels with the size of 300 mm × 200 mm were cured, they were cut at 45° orientation to produce the off-axis specimens for both open-hole and bearing strength tests. Thickness of cured composite panels ranges between 3.2 to 3.6 mm depending on the warp and weft number of layers.

3 Testing and Characterisation

3.1 Open-Hole Tension

According to the ASTM standard D5766 "Test Method for Open-Hole Tensile Strength of Polymer Matrix Composite Laminates" [23], the suggested specimen dimension is $200 \times 36 \ mm^2$ with a hole diameter of 6 mm. In this case, the diameter-to-width ratio (d/w) is 1/6. However, the suggested specimen dimension is not entirely followed here. The
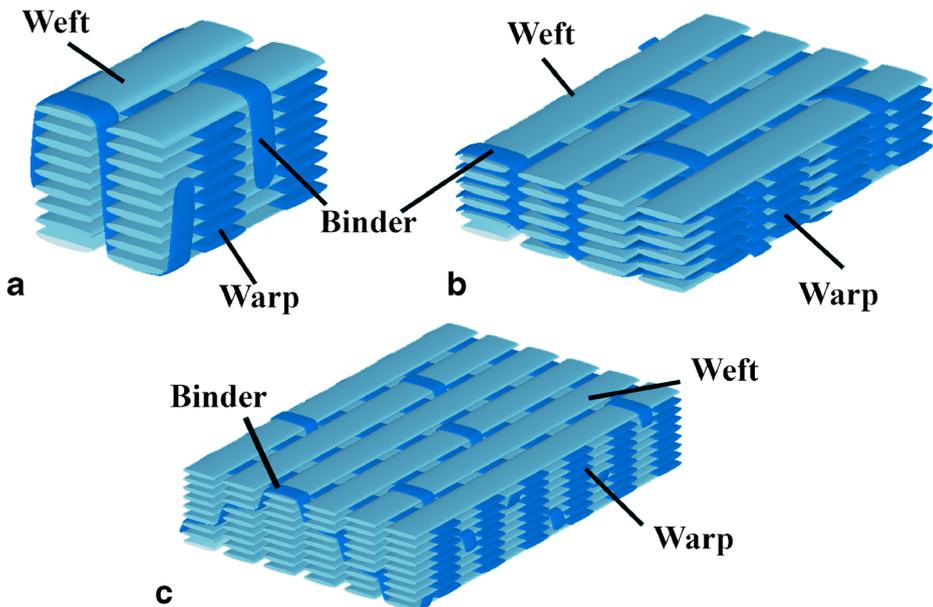
Fig. 1 Schematics of 3D woven composites: (**a**) ORT, (**b**) LTL, (**c**) AI

Table 1 Specification of textile architecture of 3D woven composites

Parameter	ORT	LTL	AI
Warp fibre count	12 k	12 k	12 k
Weft fibre count	12 k	12 k	12 k
z-binder fibre count	6 k	12 k	6 k
Ends/cm (warp)	31.52	17.73	31.52
Picks/cm (weft)	38.00	36.00	34.00
Binders/cm (z-binder)	3.94	17.73	3.94
Areal density (g/m^2)	3353	3260	3044

objective of the study is to compare the notched strength of the off-axis 3D woven specimens against the un-notched ones. Since the un-notched specimens were standard tensile coupon specimens, the nominal dimension is 250 × 25 mm^2, thus, the open-hole tensile specimens were cut with the same dimension but the ratio between the hole diameter and specimen width (d/w) was kept as 1/6 according to the standard. It is worth mentioning here that this was the only modification made to the testing method D5766.

3.1.1 Specimen Preparation

Before the drilling process, area to be drilled was 'sandwiched' between two small glass/epoxy plates with tapes in order to minimise the damage around the hole rims. The hole of 4.16 mm diameter was made by CNC lathe machine (VMX42SR, Hurco). The drilling process was carried out in water-cooled environment at 3000 rpm starting with 2 mm hole. Then, the hole was reamed until the diameter reached 4.16 mm. For Digital Image Correlation (DIC), speckle pattern was applied on the area of 50 mm × 25 mm in the middle of specimen. Two coats of white spray paint were applied on the surface. Upon drying, black paint was sprayed over the white surface forming the speckle pattern.

3.1.2 Test Setup

The open-hole tensile test was conducted, with a 2 mm/min displacement-controlled rate, for all the off-axis architectures (ORT, LTL and AI). DIC was used, as a non-contact strain measurement device, to capture the strain contour map over the specimens' surface and intensity around the hole. Figure 2 shows the test setup and the speckle pattern around the hole. Strains were acquired using DIC system utilising SensiCam 12-bit CCD camera (PCO) with TC-2336 bi-telecentric lenses (The Telecentric Company) shown in Fig. 2a. CamWare V3.11 software was used to capture the speckle pattern images (exemplified in Fig. 2b) acquired from the CCD camera. All tests were performed in a controlled environment where the temperature was 21 °C and the relative humidity (RH) was 45 %. The speckle images were then processed using Vic 2D. In processing these images, the subset size was 101 × 101 pixels. Similar settings were reported to be adequate for woven specimens [24, 25]. In addition, the step size (distance between subsets) was set to 5 pixels. The observation window of approximately 25 × 22 mm^2 produced an image with dimensions of 1040 × 896 pixels. Global mean values of strains (ε_{xx}; ε_{yy}; ε_{xy}) are obtained from DIC analysis using Vic 2D.
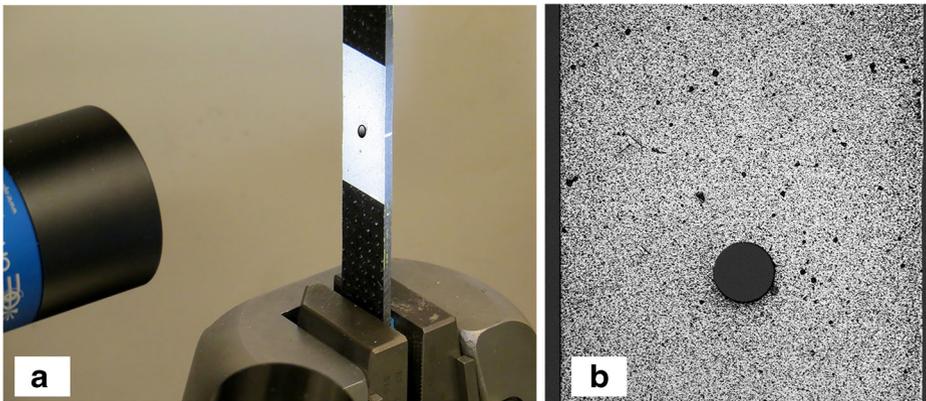
Fig. 2 Open hole tension (**a**) Test setup (the hole has been highlighted for clarification), (**b**) Typical speckle pattern around the hole

3.2 Double-Lap Bearing Strength

3.2.1 Testing Procedure

The single-fastener double-lap bearing strength test is conducted according to "*Procedure A*" of the ASTM standards D5961 "Bearing Response of Polymer Matrix Composite Laminates". The specimen dimensions are (135×36 mm^2) with a hole diameter of 6 mm and an end distance of 18 mm; so the diameter to width ratio (d/w) is (1/6). The drilling was carried out with a steel-tipped drill bit. The fastening torque applied is 2.8 N.m which is again within the recommended range of the ASTM standard (2.2 N. M to 3.4 N.m). With a 2 mm/min displacement-controlled rate, the test was conducted for all the off-axis architectures (ORT, LTL and AI). Axial Video Extensometer (AVE) was used, as a non-contact strain measurement device, to capture the strain throughout the whole test. A schematic of the test setup is shown in Fig. 3. All tests were performed in a controlled environment where the temperature was 21 °C and the relative humidity (RH) was 45 %. It is recommended by the standards to stop the test at 50 % strain in order not to mask the failure mode of the specimens. However, in this study, there was an interest in calculating the energy absorption up to final failure of the joint. Thus, five specimens were tested for ORT, LTL and AI resulting in fifteen specimens in total. Three of those five were tested only up to 50 % strain to be able to evaluate the failure mode while the other two were tested up to final failure.

3.2.2 X-Ray CT Setup

The damaged 3D woven composite samples (ORT, LTL and AI) were examined using X-ray CT. Dye penetrant was employed to enhance the contrast between damaged volume (air) and the bulk composite prior to X-ray CT imaging. The dye penetrant consisted of 250 g zinc iodide, 80 ml distilled water, 80 ml isopropyl alcohol and 1 ml Kodak photoflow. The samples were soaked in the dye penetrant solution for 24 h in order to allow sufficient penetration into all connected damage. X-ray CT scanning was performed on the Nikon XTH 225 CT scanner in Henry Moseley X-ray Imaging Facility. Tungsten target was used and the accelerating voltage and current were set to 100 kV and 70 µA respectively. The exposure time for each

Fig. 3 Schematic of double-lap bearing strength test
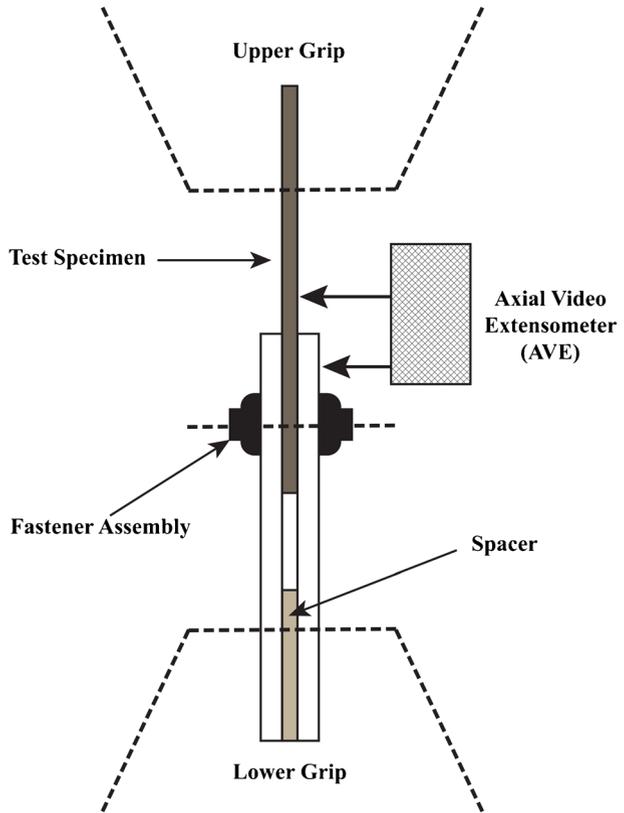
projection was 1 s and 5013 projections were collected over 360°, resulting in total data acquisition time of 1.5 h. Reconstruction was performed using the 3D CT Pro software and voxel size of the reconstructed CT datasets was $16.8 \times 16.8 \times 16.8 \ \mu m^3$. 3D visualisation and data analysis were carried out using Avizo 9.0 software.

4 Results and Discussion

4.1 Open-Hole Tension

4.1.1 Stress Strain Curves

Global stress strain curves for the notched 3D woven composites loaded in the off-axis direction are shown in Fig. 4a-c. For the sake of comparison, the open-hole "notched" results are plotted in dashed line format against the un-notched results in solid lines. For all the tested architectures, the linear elastic behaviour of the notched curve is almost the same as the un-notched or at least lies within the experimental marginal error. Once damage accumulates after the "knee" point, there is a slight reduction in the slope of the ORT notched result compared to the un-notched ones. However, for the LTL and AI architectures, this difference is not significant. The ultimate
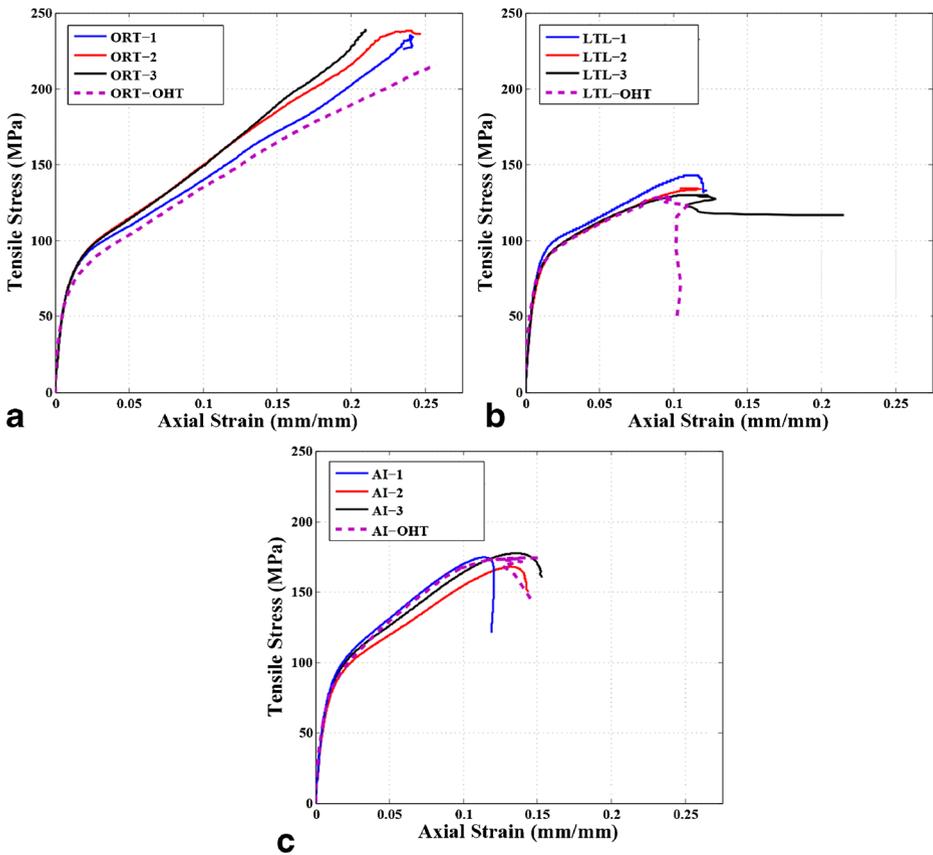
Fig. 4 Stress strain curves for un-notched "solid" vs. notched "dashed" lines for (**a**) ORT, (**b**) LTL, (**c**) AI

tensile strength mean values for the notched and un-notched specimens are detailed in Table 2. For all the tested architectures, the normalised notched tensile strength is greater than 90 % of the un-notched ultimate strength. This suggests that the 3D woven architectures in the off-axis orientation are relatively less sensitive to the notches existence. Further understanding of the damage progression and reasons for this notch insensitivity is discussed in detail later in this section.

To evaluate the notch sensitivity of the tested off-axis 3D woven composites "at this specific hole diameter to width ratio", the notched tensile strength is normalised by the un-notched strength. Then, the normalised value is compared against the ideally ductile "notch insensitive" curve and the ideally brittle "notch sensitive" curve as depicted in Fig. 5.

Table 2 Comparison between average notched and un-notched strength for 3D woven architectures loaded off-axially

Textile architecture	Strength Un-notched (MPa)	Strength Notched (MPa)	σ_n/σ_{un}
ORT	237.37	215.29	0.91
LTL	135.73	128.31	0.95
AI	173.3	172.21	0.99

Fig. 5 Notch sensitivity/
normalised strength in off-axis
composites
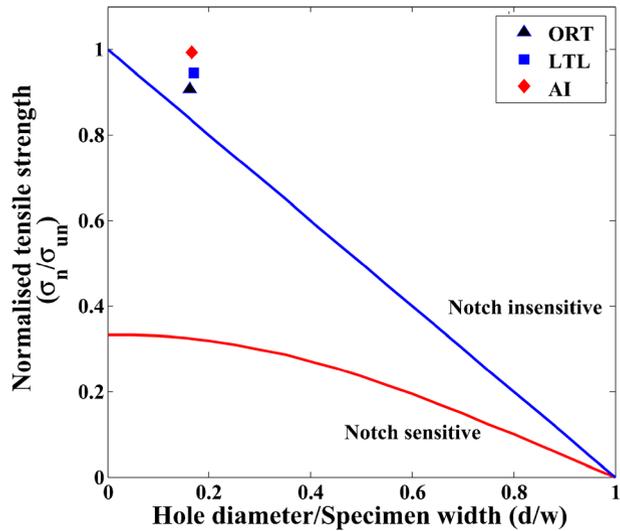
Equations for calculating the notch sensitive and notch insensitive responses [26] are detailed as follows:

- Notch insensitive (ductile materials)

$$\sigma_n/\sigma_{un} = 1-(D/W) \tag{1}$$

Where:

(σ_n) The notched tensile strength
(σ_{un}) The un-notched tensile strength
(D) The hole diameter
(W) The specimen width
- Notch sensitive (brittle materials)

$$\sigma_n/\sigma_{un} = [1-(D/W)]/K_T \tag{2}$$

Where:

$$K_T = 2 + [1-(D/W)]^3 \tag{3}$$

It is clear from the comparison shown in Table 2 that all the three 3D woven architectures are notch insensitive when loaded in the off-axis orientation for this specific diameter to width ratio. This behaviour can be attributed to two reasons. The first reason is common even for laminated composites which is the lay-up orientation in that case. And the fact that the tested architectures are 3D woven composites is not significantly affecting the behaviour. However, the second reason is the effect of the binder existence which typically distinguishes 3D woven composites from their 2D laminated counterparts. To elaborate more on those two reasons, the change of the lay-up orientation from (0/90) to (±45) directly affects the Stress Concentration

Factor (SCF) at the notch "hole". For an isotropic material, the SCF of a hole in an infinite plate [27] is approximately 3. Composites are not isotropic in nature; actually they are anisotropic material systems in which the material response is completely dependent on the lay-up. For orthotropic laminates loaded at an angle from their principal directions [1], the SCF varies between (0 to 8) times the global stress applied. This is explained further by applying the stress transformation tensor to the global stress taking into consideration the angle between the loading direction and the lamina principal directions. The off-axis (±45) orientation reduces the global stress concentration to approximately 1.7 times the global stress; which means less sensitivity to the notch "hole" presence. In addition, 3D woven composites are characterised by out-of-plane binding yarns that holds the in-plane yarns. In the case of notched specimens those binding yarns play a major role in supressing delamination and damage evolution as well as stress redistribution on wider areas as reported previously in [25] and will be elaborated more in the following section.

Remark:

- The relative notch "size/diameter" to the unit-cell size of 3D woven architectures is an important parameter that should be investigated as it may affect the response of those material systems. Due to material shortage, only one notch size was considered in this study and it was less than the unit-cell size for all architectures ORT, LTL and AI.

4.1.2 Damage Evolution

Analysis of the DIC images Figs. 6, 7 and 8 better explains the strain/ stress distribution and damage evolution in all the notched 3D woven architectures loaded in the off-axis direction at various loading levels. At the very early loading levels ~5 % strain (Figs. 6a, 7a and 8a), the strain distribution shows that the localised strain/stress regions do not only exist around the hole edge but also at the interlacement points between the binding yarns and the weft yarns of the 3D woven composites. Regions of localised strain in all architectures lie on the (±45°) directions.

When the load is increased, the stress concentration regions in all the architectures can be found only at the notch "hole" tip. This is clear in (Figs. 6b, 7b and 8b) where the red regions are highlighted. Due to this stress concentration, damage and cracking initiates in the form of matrix cracking. Although at that stage the global strain applied does not exceed 10 %, very high strain values (> 25 %) is observed around the hole edge which indicates the regions of stress concentration and eventually the premature damage. It is worth mentioning here that those strain/stress concentration regions captured by the DIC suggests that the level of damage is even higher than the induced damage due to the free-edge cracking at that stage of loading.

Upon load increase, the damage zone expands along the (±45) direction (Figs. 6c, 7c and 8c) in the form of matrix cracking and delamination until they are arrested by binding yarns. This is one major difference in the damage evolution between 3D woven and laminated composites. In laminated composites, those (±45) matrix cracking and delamination extend across the specimen width and lead to final fracture of the specimens in an instantaneous catastrophic manner [26] while in 3D woven composites, the damage evolution is more progressive damage and does not lead to catastrophic fracture. Finally before failure (Figs. 6d, 7d and 8d), the ORT architecture is different from the other architectures in the sense that strain/stress is redistributed
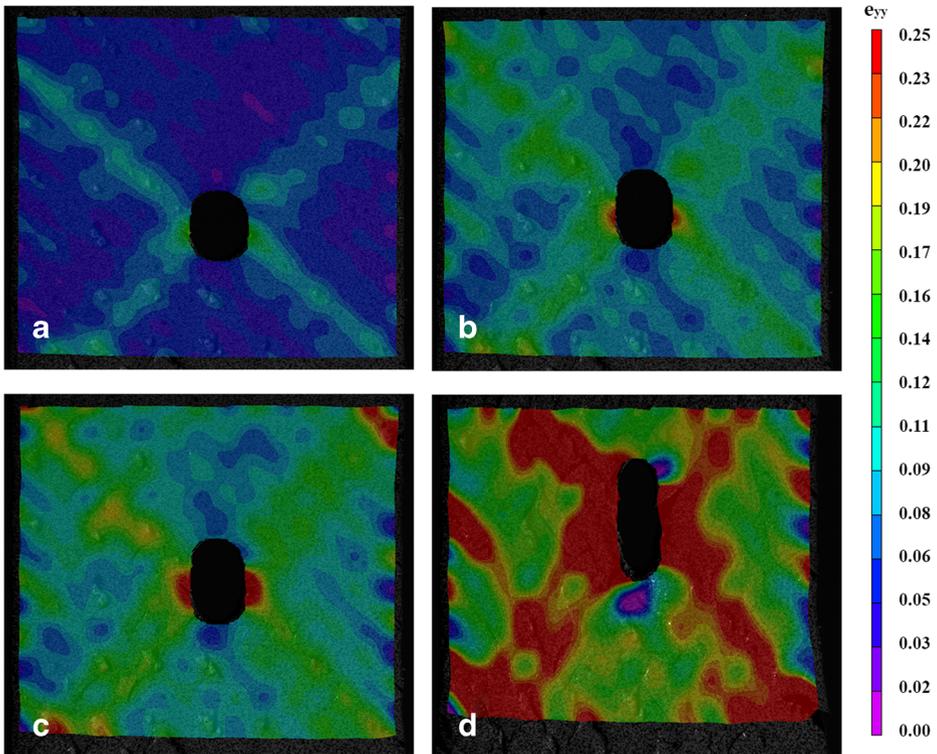
Fig. 6 Evolution of axial strain contour map for ORT (**a**) 0.05, (**b**) 0.09, (**c**) 0.11, (**d**) 0.18 mean strain

over a larger area of the specimen unlike the AI and LTL where the damage spans along a (±45) degree line and causes final fracture without being arrested by the binders. To be more precise, damage progression and cracking cause the binder to fracture which leads to the final failure of those architectures. Through the whole test, the hole elongation is properly captured by the DIC system as shown in (Figs. 6, 7 and 8).

Optical images for the surfaces of the three tested architectures (Fig. 9a-c), just right before fracture, demonstrate excessive hole elongation, matrix cracking and inter-yarn delamination in the form of ply separation and free-edge cracking around the hole and at the edges of the specimens. Again, it is clear that due to the higher binders density in the ORT architecture, the matrix cracking and delamination are arrested and do not extend along the whole span of the specimens' width as is the case in the LTL and AI architectures.

4.2 Double-Lap Bearing Strength

4.2.1 Stress Strain Curves

The global bearing stress/bearing strain curves for the 3D woven composites loaded in the off-axis direction, up to 50 % strain, are shown in Fig. 10a-c. The initial portion of the bearing stress/bearing strain curves, for all architectures, exhibits a non-linear behaviour which is
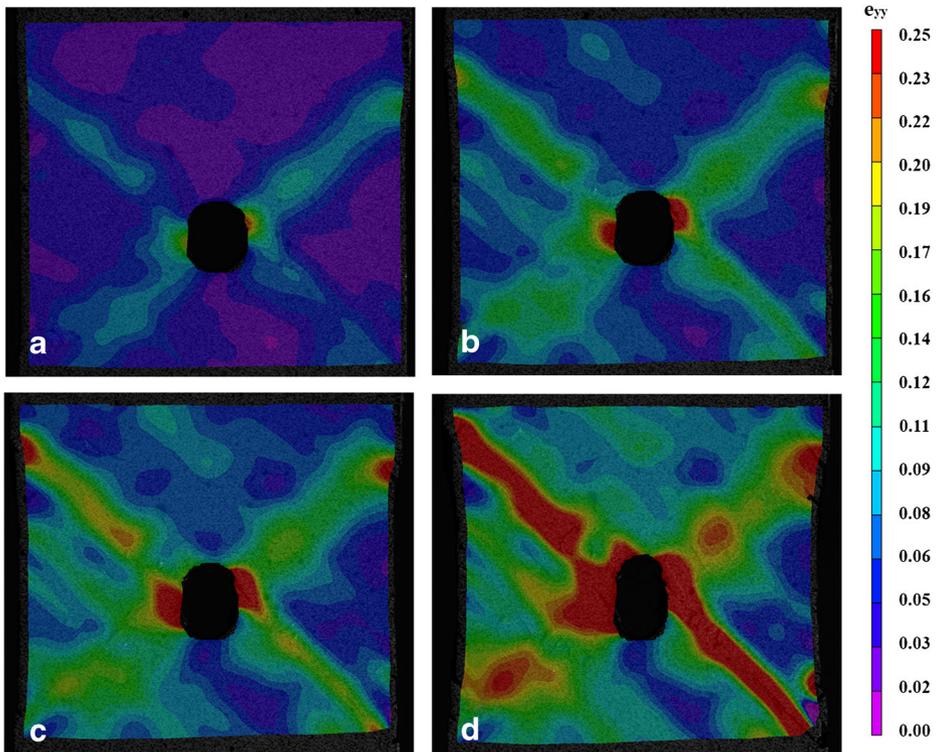
Fig. 7 Evolution of axial strain contour map for LTL (**a**) 0.04, (**b**) 0.07, (**c**) 0.09, (**d**) 0.12 mean strain

correlated, in the ASTM D5961 standard [28], to a combination of different factors, which include joint translation due to the hole tolerance, joint straightening and joint friction. That is why the bearing stiffness has to be determined beyond this effect in the linear portion of the curve. Once the stiffness is determined, the effective strain origin is the intersection of the chord stiffness line with the bearing strain axis. This effective strain origin is then used to calculate the offset bearing strength. The reader is referred to the ASTM standard [28] for detailed discussion of results and calculations. There is no significant difference in the global behaviour of the three tested architectures up to 50 % strain. The bearing stress/bearing strain curve is characterised by linear response up to a specific strain where a drop in the stress is observed. Then, the bearing stress continues increasing with a lower slope with increasing applied strain up to a maximum stress value which represents the ultimate bearing strength.

Table 3 summarises the bearing stiffness, offset bearing strength and ultimate bearing strength values for ORT, LTL and AI. It is clear from the comparison that the bearing stiffness of ORT is less than AI and LTL. This may be due to ORT architecture having the highest z-binder density and smaller unit cell size. However, no significant difference is observed for either the offset bearing strength or the ultimate bearing strength. As specimens are loaded in the off-axis orientation, it is useful to compare the ultimate bearing strength with the compressive strength of the same material systems along the warp and weft directions.
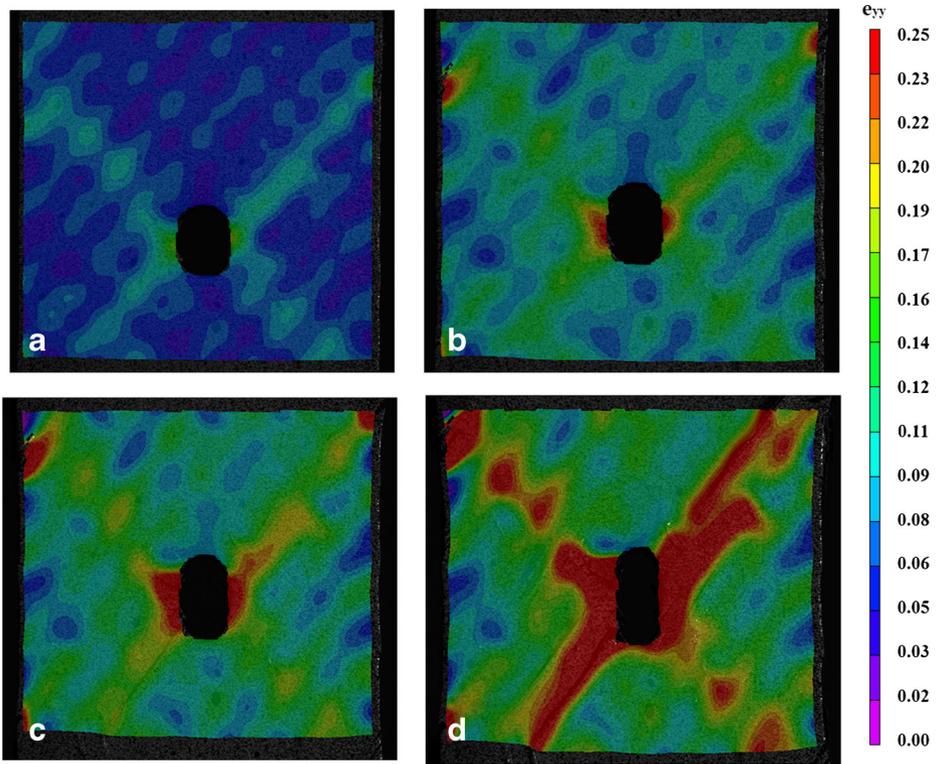
Fig. 8 Evolution of axial strain contour map for AI (**a**) 0.06, (**b**) 0.10, (**c**) 0.12, (**d**) 0.15 mean strain

The 2D stress transformation for a plane-stress case (see Fig. 11a) is used here to transform the global (x, y) ultimate bearing strength into the local "warp and weft" directions (1, 2).

$$\begin{Bmatrix} \sigma_1 \\ \sigma_2 \\ \tau_{12} \end{Bmatrix} = [T_1] \begin{Bmatrix} \sigma_x \\ \sigma_y \\ \tau_{xy} \end{Bmatrix} \tag{4}$$

where $[T_1]$ is the stress transformation matrix (a second-order tensor)
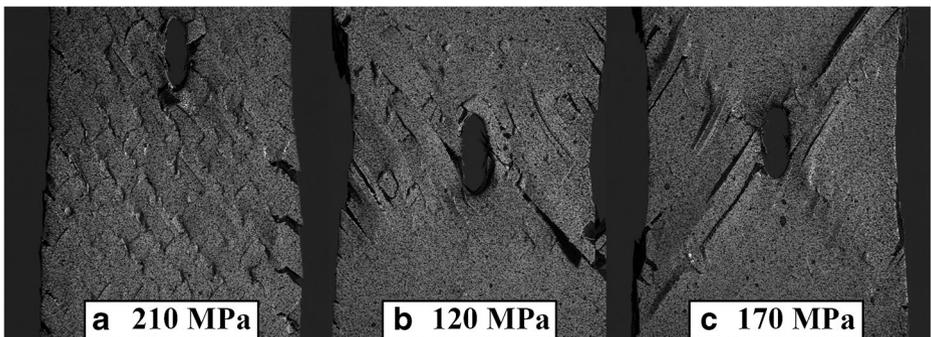
Fig. 9 Optical surface images at failure for (**a**) ORT, (**b**) LTL, (**c**) AI
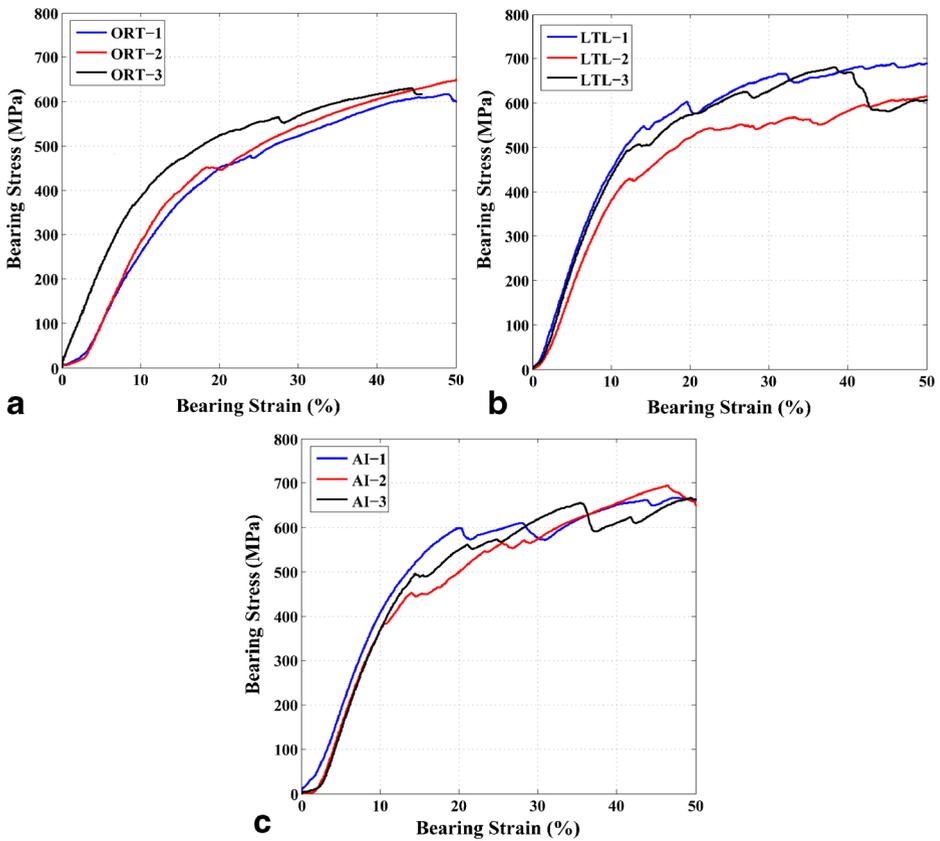
Fig. 10 Bearing stress vs. bearing strain curves up to 50 % strain for (**a**) ORT, (**b**) LTL, (**c**) AI

$$[T_1] = \begin{bmatrix} m^2 & n^2 & 2mn \\ n^2 & m^2 & -2mn \\ -mn & mn & m^2-n^2 \end{bmatrix} \tag{5}$$

where: $m = \cos(\theta)$, $n = \sin(\theta)$ and $\theta = 45^o$. Substituting Eq. 5 equation into Eq. 4 leads to the following system of equations (Eq. 6) for the stresses in principal "local" coordinate system which are the warp and weft directions respectively.

$$\begin{aligned} \sigma_1 &= m^2\sigma_x + n^2\sigma_y + 2mn\tau_{xy} \\ \sigma_2 &= n^2\sigma_x + m^2\sigma_y - 2mn\tau_{xy} \\ \tau_{12} &= -mn\sigma_x + mn\sigma_y + (m^2-n^2)\tau_{xy} \end{aligned} \tag{6}$$

Table 3 Summary of bearing stiffness and strength for ORT, LTL and AI

Textile architecture	Bearing stiffness (GPa)	Offset bearing strength (MPa)	Ultimate bearing strength (MPa)
ORT	3.48 ± 0.02	429.63 ± 57.53	658.67 ± 27.62
LTL	5.32 ± 0.23	466.97 ± 33.06	677.33 ± 22.95
AI	5.26 ± 0.09	456.90 ± 38.33	683.33 ± 9.39
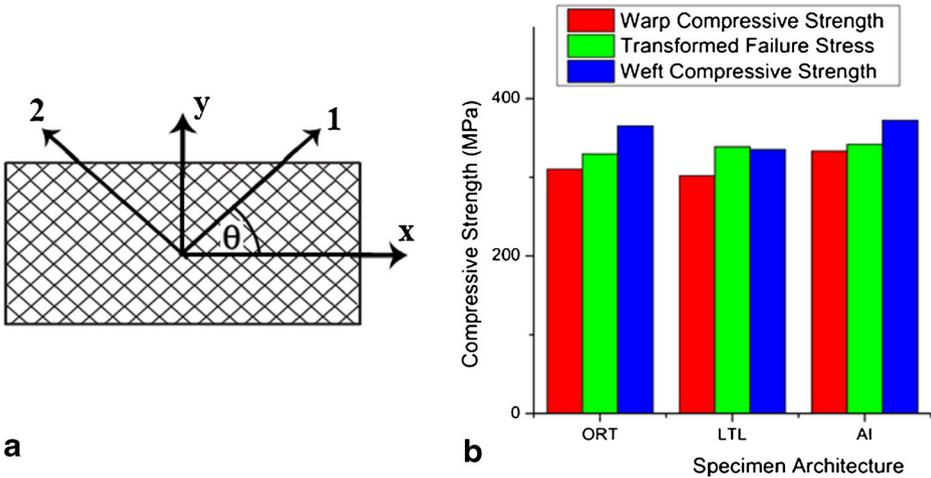
Fig. 11 Transformed bearing strength: (**a**) schematic of coordinate system transformation, (**b**) comparison with compressive strength in warp and weft directions

In the case of bearing strength test, the global applied load is only axial ($\sigma_x \neq 0$) which reduces Eq. 6 to Eq. 7 in the local coordinate system (1, 2) as follows:

$$
\begin{aligned}
\sigma_1 &= m^2 \sigma_x \\
\sigma_2 &= n^2 \sigma_x \\
\tau_{12} &= -mn\sigma_x
\end{aligned} \tag{7}
$$

Then, the transformed stress obtained are compared against the ultimate compressive strength (see Fig. 11b) of the same material systems tested experimentally along the warp and the weft directions in a standard compression test according to ASTM D3410 "Compressive Properties of Polymer Matrix Composite Materials with Unsupported Gage Section by Shear Loading". For all the tested architectures, the stress at failure in the local coordinate system "warp/weft" exceeds the strength of the material either in the warp or the weft directions (see Table 4).

The next step was to investigate the bearing response of ORT, LTL and AI up to final failure. Global bearing stress/ bearing strain curves are depicted in Fig. 12. Although there is no significant difference between all the architectures up to 50 % strain, the response is different up to failure. It is obvious that the LTL architecture fails first (~85 % strain) followed by the AI (~105 % strain) and finally ORT (~140 % strain). This higher strain to failure is associated with higher energy absorption for ORT (~760 MJ/m³) as opposed to AI (~590 MJ/m³) and finally LTL (~490 MJ/m³). This suggests that the damage progression is different depending on the 3D

Table 4 Comparison of transformed bearing strength against warp and weft compressive strength for ORT, LTL and AI

Textile architecture	Warp compressive strength (MPa)	Transformed bearing strength (MPa)	Weft compressive strength (MPa)
ORT	310 ± 4.18	329.33 ± 13.81	365.33 ± 4.5
LTL	302 ± 26.9	338.67 ± 11.48	335 ± 27.3
AI	333 ± 22.4	341.67 ± 4.70	372 ± 54.42
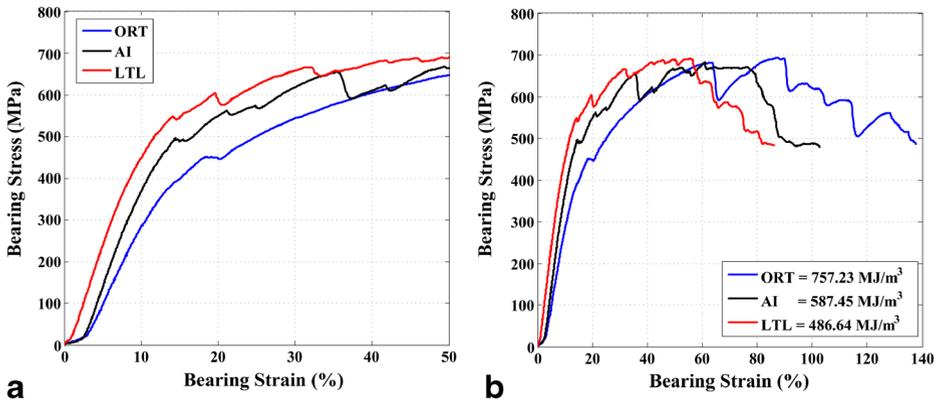
Fig. 12 Bearing stress vs. bearing strain: (**a**) up to 50 % strain, (**b**) up to failure

woven architecture. A similar trend was reported in [25] for testing 3D woven composites in tension in the off-axis direction. The smaller unit cell size (higher z-binder density) in ORT redistributes the stress over a wider region of the specimen and resists cracking and delamination progression. Further understanding of the damage mechanisms is thus studied using X-ray CT and is reported in the following section.

4.2.2 X-Ray CT Damage Characterisation

To assess the level of damage and various damage mechanisms in the double-lap bearing strength test, X-ray CT was used. Specimens tested up to 50 % strain are scanned, as detailed in Section 3.2.2. To aid the damage analysis using X-ray CT, nomenclature of damage types is given in Table 5. A comparison between the damaged specimens and the X-ray front view for ORT, LTL and AI is shown in Fig. 13. Although damage is not very obvious on the surface of the specimens, the X-ray images reveal more information. All specimens fail in a bearing failure mode (B-type) which is highlighted by the rectangular dashed frame (see Fig. 13d-f). Clear yarns distortion is experienced by the LTL architecture at the hole front tip (see Fig. 13b, e) while it is less severe in ORT (see Fig. 13a) and AI (see Fig. 13c). Transverse cracking (T-type) dominates the three architectures ORT, LTL and AI. However, the propagation length of the cracks seems to be architecture dependent, specifically, unit cell size dependent. Transverse cracks propagates along the yarn longitudinal direction until it reaches a z-binder yarn; so the least cracking length is observed in ORT, followed by LTL and then AI. Once transverse

Table 5 Nomenclature of damage types in bearing strength test	Code	Damage type
	F	Free edge matrix crack between yarns
	Z	Z-binder induced damage
	T	Transverse crack within yarns
	D	Inter-yarn matrix delamination
	M	Matrix damage
	B	Bearing Failure
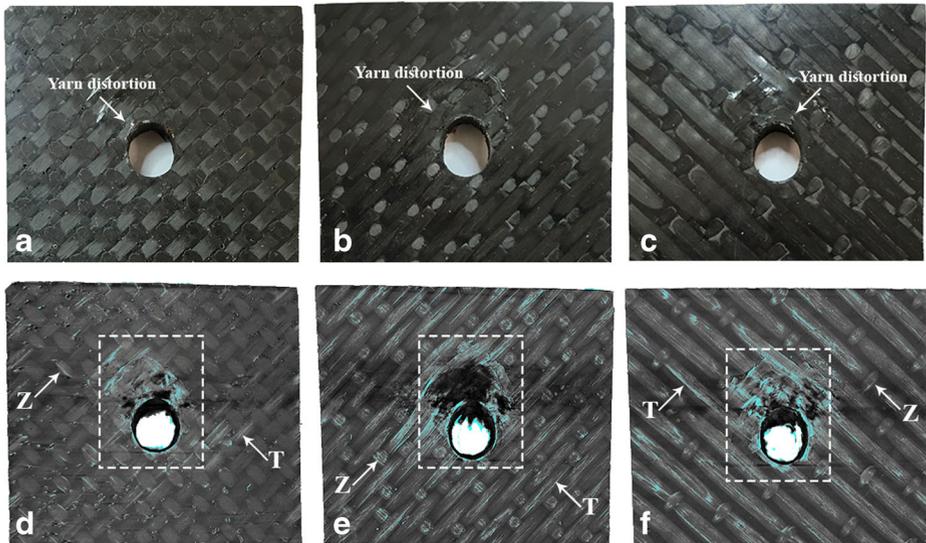
Fig. 13 At 50 % strain: (**a**, **b**, **c**) damaged specimens, (**d**, **e**, **f**) X-ray front view for ORT, LTL and AI respectively

cracking is suppressed by the z-binder yarns, another damage mechanism is observed in the form of z-binder induced damage (Z-type).

After reconstruction of the 2D scanned slices, the 3D volume of the damage specimens is visualised in (Fig. 14b–f). The size of the B-type damaged region is the largest in the LTL architecture, smaller in AI and the smallest in ORT. Although all specimens are deformed with the same strain level, Fig. 14b–f suggests that ORT has the highest resistance to deformation followed by AI and finally LTL. This supports the argument that the smaller unit cell size of the ORT fibre architecture (higher z-binder density) redistributes the stress over a wider region and resists cracking and delamination propagation.

The next step is to virtually cut a sectioning plane along the warp direction to reveal the damage along the z-binder path (see Fig. 14b–f) in the 3D reconstructed volume. In all architectures, bearing failure with extensive matrix crushing and damage (type-M) is observed at the hole periphery in the loading direction "bearing plane". In addition, free edge cracking (type-F) is common in all architectures. In case of ORT (see Fig. 14a) and AI (see Fig. 14e), the through-thickness binder prevents the delamination (type-D) from growing across the width of the specimen. On the contrary, the z-binding yarns in LTL (see Fig. 14c) guide the delamination (type-D) along their path. In regions where z-binding yarns do not exist, delamination (type-D) grows across the specimen width, even in ORT and AI architectures. This indicates that the z-binder architecture plays a major role in determining the damage path in 3D woven composites and consequently their damage resistance and global stress/strain response.

5 Concluding Remarks

The notched response of 3D woven composites, in the off-axis orientation, has been studied by open hole tension and double-lap bearing strength tests. For open hole test, the global stress
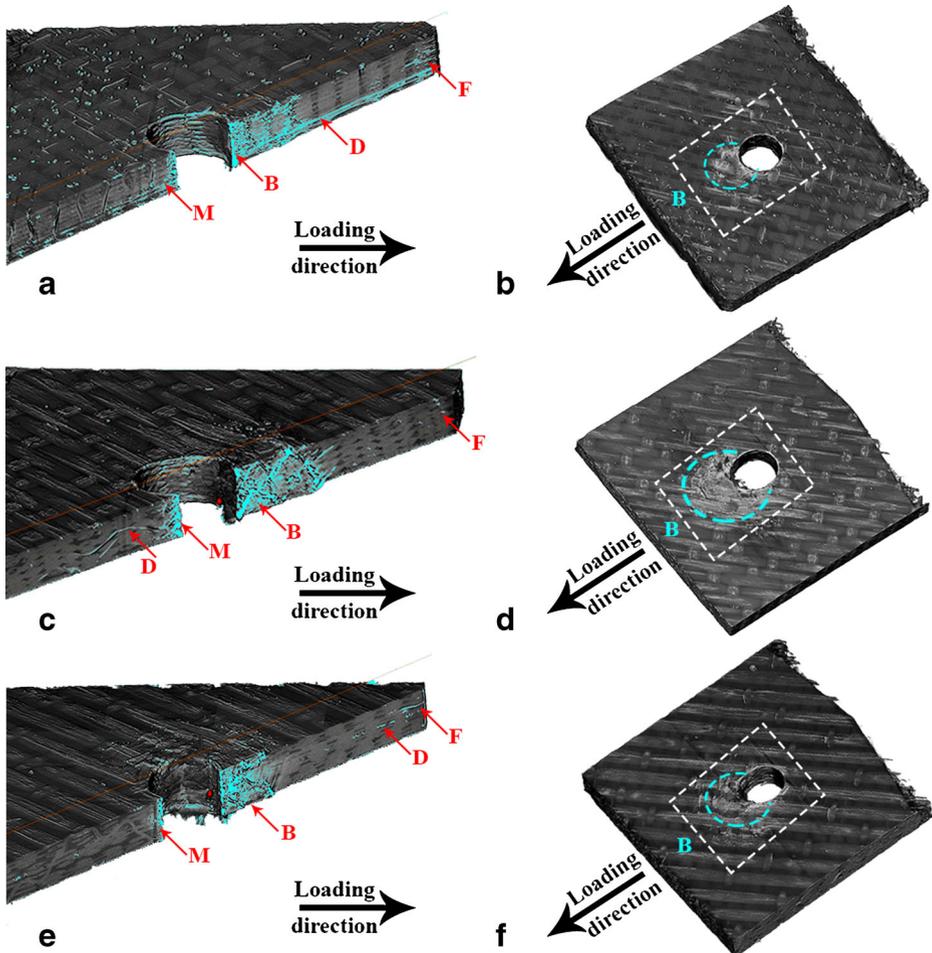
Fig. 14 X-ray CT scans: (**a**, **c**, **e**) virtual sectioning along the warp direction, (**b**, **d**, **f**) isometric 3D volume for ORT, LTL and AI respectively

strain response suggests that all 3D woven architectures (ORT, LTL, and AI) are notch insensitive. The final failure of all the 3D woven architectures in the off-axis direction is progressive failure not catastrophic brittle fracture. Out of all the tested architectures, ORT architecture in the off-axis orientation exhibits higher ultimate strength and strain to failure as it was the case for the un-notched specimens. From the DIC analysis, the ORT architecture redistributes the stress over a wider region away from the hole which reduces the stress concentration at the notch periphery. In addition, the higher intensity of binding yarns acts as crack stoppers for delamination and matrix cracking. For double-lap bearing strength test up to 50 % strain, no significant variation in the global bearing stress/bearing strain response was observed as all of them failed in a bearing failure mode. However, X-ray CT damage characterisation revealed the effect of the z-binder architecture on the damage mechanisms and delamination propagation. The dominant damage mechanisms include matrix crushing, extensive delamination, transverse cracking and z-binder induced damage. Loading specimens

up to failure showed that the ORT architecture in the off-axis direction resists deformation and damage progression followed by AI and finally LTL. This suggested that in addition to the unit cell size effect, having a through-thickness binder (ORT and AI) can suppress delamination and delay final failure. On the contrary, delamination progression is guided by the z-binding yarns between layers which led to final failure of LTL architecture. This is reflected on the energy absorption of ORT being the highest, followed by AI and finally LTL. Thus, 3D woven composites in the off-axis orientation, especially ORT, demonstrate a potential of overcoming some of the major challenges facing composite joints' applications which are: high energy absorption, stress redistribution away from the notch and notch insensitivity.

References

1. Jones, R.: Mechanics of composite materials. (1998)
2. Kelly G.: Load transfer in hybrid (bonded/bolted) composite single-lap joints. Compos. Struct. **69**, 35–43 (2005)
3. Sun C.T., Luo J.: Failure loads for notched graphite/epoxy laminates with a softening strip. Compos. Sci. Technol. **22**, 121–133 (1985)
4. Awerbuch J., Madhukar M.S.: Notched strength of composite laminates: predictions and experiments & mdash - a review. J. Reinf. Plast. Compos. Reinf. **4**, 3–159 (1985)
5. Wang J., Callus P.J., Bannister M.K.: Experimental and numerical investigation of the tension and compression strength of un-notched and notched quasi-isotropic laminates. Compos. Struct. **64**, 297–306 (2004)
6. Yudhanto A., Watanabe N., Iwahori Y., Hoshi H.: The effects of stitch orientation on the tensile and open hole tension properties of carbon/epoxy plain weave laminates. Mater. Des. **35**, 563–571 (2012)
7. Yudhanto A., Iwahori Y., Watanabe N., Hoshi H.: Open hole fatigue characteristics and damage growth of stitched plain weave carbon/epoxy laminates. Int. J. Fatigue. **43**, 12–22 (2012)
8. Naik N.K., Shembekar P.S., Verma M.K.: On the influence of stacking sequence on notch sensitivity of fabric laminates. J. Compos. Mater. **24**, 838–852 (1990)
9. Shembekar P.S., Naik N.K.: Notched strength of fabric laminates. II: Effect of stacking sequence. Compos. Sci. Technol. **44**, 13–20 (1992)
10. Cox B.N., Dadkhah M.S., Morris W.L.: On the tensile failure of 3D woven composites. Compos. Part A Appl. Sci. Manuf. **27**, 447–458 (1996)
11. Tsai K.H., Chiu C.H., Wu T.H.: Fatigue behavior of 3D multi-layer angle interlock woven composite plates. Compos. Sci. Technol. **60**, 241–248 (2000)
12. Dai S., Cunningham P.R., Marshall S., Silva C.: Open hole quasi-static and fatigue characterisation of 3D woven composites. Compos. Struct. **131**, 765–774 (2015)
13. Mubeen, A.: Damage Tolerance of 3D Woven Composites with Weft Binders. (2014).
14. Ataş A., Soutis C.: Strength prediction of bolted joints in CFRP composite laminates using cohesive zone elements. Compos. Part B Eng. **58**, 25–34 (2014)
15. Ataş A., Soutis C.: Subcritical damage mechanisms of bolted joints in CFRP composite laminates. Compos. Part B Eng. **54**, 20–27 (2013)
16. Atas, A.: Strength Prediction of Mechanical Joints in Composite Laminates Based on Subcritical Damage Modelling. (2012)
17. Kelly G., Hallström S.: Bearing strength of carbon fibre/epoxy laminates: effects of bolt-hole clearance. Compos. Part B Eng. **35**, 331–343 (2004)

18. Khashaba U.A., Sebaey T.A., Alnefaie K.A.: Failure and reliability analysis of pinned-joints composite laminates: Effects of stacking sequences. Compos. Part B Eng. **45**, 1694–1703 (2013)
19. Öndürücü A., Esendemir Ü., Tunay R.F.: Progressive failure analysis of glass-epoxy laminated composite pinned-joints. Mater. Des. **36**, 617–625 (2012)
20. Pisano A.A., Fuschi P.: Mechanically fastened joints in composite laminates: Evaluation of load bearing capacity. Compos. Part B Eng. **42**, 949–961 (2011)
21. Thoppul S.D., Finegan J., Gibson R.F.: Mechanics of mechanically fastened joints in polymer-matrix composite structures - a review. Compos. Sci. Technol. **69**, 301–329 (2009)
22. Warren K.C., Lopez-Anido R.A., Goering J.: Behavior of three-dimensional woven carbon composites in single-bolt bearing. Compos. Struct. **127**, 175–184 (2015)
23. ASTM D5677: Standard Test Method for Open-Hole Tensile Strength of Polymer Matrix Composite. (2013)
24. Saleh M.N., Lubineau G., Potluri P., Withers P.J., Soutis C.: Micro-mechanics based damage mechanics for 3D orthogonal woven composites: experiment and numerical modelling. Compos. Struct. **3–12**, (2016)
25. Saleh, M.N., Yudhanto, A., Potluri, P., Lubineau, G., Soutis, C.: Characterising the loading direction sensitivity of 3D woven composites: effect of z-binder architecture. Compos. Part A Appl. Sci. Manuf. **90**, 577–588 (2016)
26. Callus P.J.: The effects of hole-size and environment on the mechanical behaviour of a quasi-isotropic AS4 / 3501–6 laminate in tension. Compression and bending. DSOT (Defence Science and Technology Organization) Austrlaian Government Department of Defence, Victoria. http://dspace.dsto.defence.gov.au/dspace/handle/1947/9030 (2007). Accessed 11 April 2016
27. Yang Q.Q., Gao C.F., Chen W.T.: Stress concentration in a finite functionally graded material plate. Sci. China Phys. Mech. Astron. **55**, 1263–1271 (2012)
28. ASTM D5961: Standard Test Method for Bearing Response of Polymer Matrix Composite Laminates. (2003)